ACS Photonics

Article

Cite This: ACS Photonics 2017, 4, 2419-2424

pubs.acs.org/journal/apchd5

Plasmon-Induced Accelerated Exciton Recombination Dynamics in ZnO/Ag Hybrid Nanolasers

Junfeng Lu,[†,‡,§] Mingming Jiang,[§,∥,⊥] Ming Wei,[†,§] Chunxiang Xu,[*,†] Shufeng Wang,[∥,⊥] Zhu Zhu,[†] Feifei Qin,[†] Zengliang Shi,[†] and Caofeng Pan[‡]

[†]State Key Laboratory of Bioelectronics, School of Biological Science and Medical Engineering, Southeast University, Nanjing 210096, China

[‡]Beijing Institute of Nanoenergy and Nanosystems, Chinese Academy of Sciences, Beijing 100083, People's Republic of China

[∥]State Key Laboratory of Luminescence and Applications, Changchun Institute of Optics, Fine Mechanics and Physics, Chinese Academy of Sciences, Changchun 130033, China

[⊥]Institute of Modern Optics and State Key Laboratory for Mesoscopic Physics, School of Physics, Peking University, Beijing 100871, China

S *Supporting Information*

ABSTRACT: The recent development of plasmonics has break through the optical diffraction limit and realized ultracompact nanolasers that can directly generate coherent optical fields at the nanometre scale. However, it remains to a profound understanding on the light and matter interactions in so-called Spaser, especially on the coupling mechanism between the surface plasmon and exciton although many reports have claimed surface plasmonic lasers. Here, we demonstrated a ZnO/SiO_2/Ag structural hybrid plasmonic nanolaser and compared with a conventional photonic laser systematically. We proposed that these two kinds of lasers originated from the entirely different optical gain mechanisms, and resulted in the generation of lasing mode shift. Time-resolved spectra collected from these two samples at room temperature presented the dynamic process of exciton recombination and revealed the energy-transfer from excitons to SPs. Our research provides an important theoretical and experimental basis for the practical application of plasmonic nanolasers in the future.

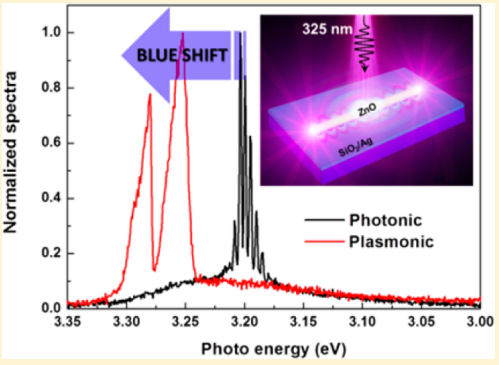

KEYWORDS: *nanolaser, surface plasmon polariton, ZnO nanorod, silver film, ultrafast optical spectroscopy*

Surface plasmon polariton (SPP) is a critical concept to break down the optical diffraction limit through storing optical energy into free-electron collective oscillations at the metal−dielectric interfaces.[1−3] It provides an ideal approach to design the novel nanodevices and realize all-optical integration for their potential application in optics communication,[4−6] biosensing,[7−9] and nonlinear optical switching.[10] Due to its unprecedented capability to generate extremely intense optical fields in the deep-subwavelength regime, surface plasmon amplification by stimulated emission of radiation (Spasers) has attracted considerable interest recently.[11−25] In comparison to the conventional photonic laser, the plasmonic cavities exhibit ultrasmall modal volume $V_m \sim \lambda^3/10 - \lambda^3/1000$ enabling the tailoring of the strong light-matter interaction in a variety of linear ($\sim Q/V_m$) and nonlinear ($\sim Q^2/V_m$ or $\sim Q/V_m^{1/2}$) optical process, where λ and Q are wavelength and the cavity quality factor, respectively. Many research works about plasmonic lasers have been reported and made sufficient progress to decrease the optical loss, reduce the laser threshold, and increase the operation temperature toward practical applications. In particular, several devices now operate at room temperature[17] and even under electrical injection.[18,19] For instance, Zhang et al.[20] theoretically proposed a hybrid dielectric waveguide with plasmonics by inserting an insulating gap layer between an optical gain medium and a metallic layer to overcome the intrinsic ohmic losses of metals. Subsequently, they achieved the experimental demonstration of nm-scale plasmonic lasers with optical modes of 100× smaller than the diffraction limit.[21] Recently, Xiong et al.[22] reported the first strong room temperature ultraviolet (~370 nm) SPP lasers consisting of GaN nanowire and aluminum film, with extremely low thresholds (~3.5 MW/cm^2) based on a closed-contact planar semiconductor−insulator−metal structure, promoting the efficient exciton-SP energy transfer and offering adequate optical gain to compensate the loss. Chou et al.[23] demonstrated a high-operation-temperature ZnO plasmonic nanolaser directly placed on as-grown single-crystalline aluminum film with a threshold of 20 MW/cm^2. In addition, Oulton et al.[24] observed a blue-shift of ZnO/Ag hybrid plasmonic mode with the pulses shorter than 800 fs compared with a conventional photonic laser. Liu et al.[25] presented a demonstration of

Received: May 10, 2017
Published: September 26, 2017

DOI: 10.1021/acsphotonics.7b00476
ACS Photonics 2017, 4, 2419−2424

utilizing the surface plasmon polariton (SPP) enhanced Burstein–Moss (BM) effect to tune the lasing wavelength of a single semiconductor nanowire by decreasing the dielectric layer thickness from 100 to 5 nm. Although great efforts have propelled the progress in function improvement and device realization, some critical scientific issues, including optical mode shift, optical gain mechanism, and SP-exciton coupling mechanism, are still in challenge.

In this case, we propose that the origins of plasmonic and photonic light emission are quite different. The calculated results of the Mott density demonstrate that the conventional photonic ZnO laser operates here via the electron–hole plasma (EHP) mechanism, with emission energy near 3.20 eV. In contrast, the hybrid plasmonic constructed in this work operates in the vicinity of the exciton and its related phonon replica energies at room temperature, near 3.30 eV. Remarkably, we have measured time-resolved photoluminescence (TRPL) spectral response collected by an optically triggered streak camera system and analyzed the temporal dynamics process. It provides direct evidence for the effective energy-transfer channel of SP-exciton coupling and exposes its own dynamics of accelerated recombination for the hybrid plasmonic device.

RESULTS AND DISCUSSION

Structure of the Hybrid Plasmonic Nanolaser. The plasmonic nanolaser under investigation consists of an individual ZnO nanorod with the length and diameter of ~15 μm and 210 nm placed on a 5 nm thick silicon dioxide (SiO_2) spacer layer over the silver (Ag) film, as shown in Figure 1a. The insulating spacer layer affords optical confinement control and reduces the intrinsic ohmic losses of metals. Ag is adopted as the plasmonic medium due to its similar SP frequency compared with excitonic emission of ZnO with a high gain below the band-edge near 3.24 eV[29,30] (Supporting Information, Figure S4) due to either exciton–exciton scattering or optical phonon scattering ($\hbar\omega_{LO}$ = 72 meV).[31,32] To ensure the sufficient gain compensation and coupling efficiency, the thickness of the insulating layer is optimized (Supporting Information, Figure S5). The photonic lasers consisted of ZnO nanorods with the length and diameter of ~10 μm and 260 nm from the same batch of nanorod arrays directly placed on a Si/SiO_2 substrate. The confined modes propagate backward and forward along the nanorod cavity ($5<L<20$ μm), with feedback arising from modal reflection at the end-facets. Under the excitation of femtosecond laser operated at 325 nm coupled with a confocal μ-PL system (OLYMPUS BX53), the plasmonic nanolasers in Figure 1b emitted a dazzling blue-violet light captured by a camera attached to this measurement setup, as shown in the inset of Figure 1a.

The three-dimensional simulations of the hybrid plasmonic fundamental mode characteristics are performed to calculate the y component of the near-field electric field distribution $\mathbf{E}_y$ along the z axis, as shown in Figure 1c. The calculated results demonstrate that the SPP wave excited at the interface between metallic film and ZnO gain medium can propagate along the z axis direction. The electromagnetic energy is mainly confined in the insulating layer of 5 nm, and oscillates back and forth inside the hybrid cavity. Different with the conventional photonic laser, the hybrid plasmonic laser exhibits the capability to reduce optical mode far below the scale of the vacuum wavelength and generates extremely focused optical excitations.

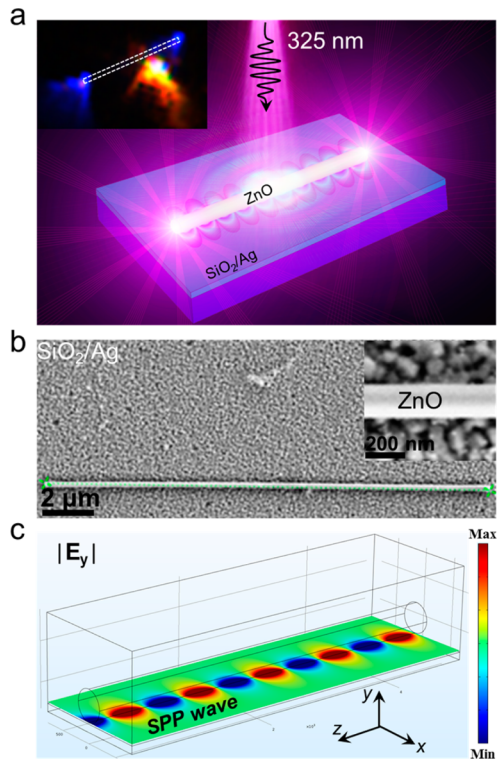

Figure 1. Schematic diagram of hybrid plasmonic nanolaser geometry and the simulated mode characteristics. (a) Schematic of a semiconductor–dielectric–metal plasmonic nanolaser optically excited with a 325 nm femtosecond laser. The inset shows a picture of a lasing plasmonic ZnO nanorod. (b) Scanning electron microscope image of a typical plasmonic laser containing a ZnO nanorod placed on the SiO_2/Ag film. (c) Three-dimensional simulation on the electric field distribution of a hybrid plasmonic fundamental mode at a wavelength of 375 nm, corresponding to ZnO X_A exciton line. The diameter and length of the gain medium are 210 nm and 4 μm, respectively. The thickness of the insulating gap is 5 nm.

Emission Polarization and Electric Field Distribution of Plasmonic and Photonic Lasing. To show the unique properties of hybridized plasmon mode, the cross-sectional electric field distribution of the plasmonic and photonic lasers are calculated by using a FDTD method, as shown in left panel of Figure 2a,b. Left panel of Figure 2b demonstrates that the hybrid plasmonic mode is strongly confined in two dimensions within the gap for a relatively small cylinder diameter ($d \approx 210$ nm) of ZnO gain medium; namely, its electromagnetic energy is mainly concentrated in the thin 5 nm insulator gap region. Conversely, the simulated result of the photonic waveguide-mode exhibits a cylinder-like mode with electromagnetic energy confined to the high-permittivity dielectric core (left panel in Figure 2a) for a large-diameter ZnO nanorod ($d \approx 260$ nm) sitting directly on the Si/SiO_2 substrate. The right panel of Figure 2a,b presents the measured far-field polarization distributions of the light emission scattered out from the nanorod end-facets. The slightly asymmetric polar plots for both of these samples could be due to the fluctuated pulse laser source and long measurement time. The mode characteristics of plasmonic and photonic nanolasers exhibit distinct polarization behavior. In the photonic device (ZnO-SiO_2), the transverse electric modes waveguide and oscillate inside the ZnO nanorod, leading to a strong lasing emission with the polarization perpendicular to the nanorod z axis (right panel of

DOI: 10.1021/acsphotonics.7b00476
ACS Photonics 2017, 4, 2419–2424

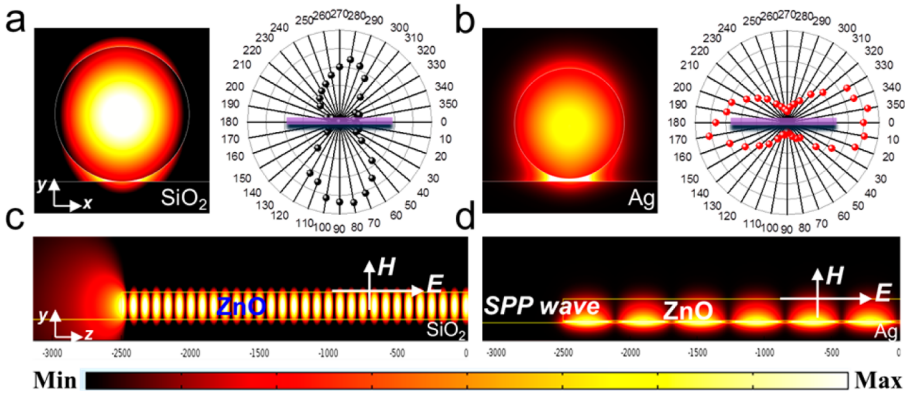

Figure 2. Measured polarization distribution and simulated electric field distribution from photonic and plasmonic nanolasers. The calculated electric field distribution in the $x-y$ plane and far-field emission intensity as a function of polarization angle collected from photonic (a) and plasmonic (b) nanolasers, consist of a 260 nm diameter ZnO rod on a SiO_2 substrate and a 210 nm diameter ZnO rod on an Ag/SiO_2 (500/5 nm) film, respectively. The polarization angle is defined as the angle between electric field direction and nanorod z axis. (c) Resonant standing-wave pattern of the photonic waveguide-mode propagating along ZnO nanorod in the $y-z$ plane. (d) Hybrid plasmonic fundamental mode field distribution along the ZnO nanorod in the $y-z$ plane, confined at the interface of ZnO/Ag.

Figure 2a). In contrast, in plasmonic device (ZnO-SiO_2-Ag), the electric field normal to the metal surface exhibits the strongest coupling to SPP, which results in the emission with the polarization parallel to the nanorod z axis direction. In order to display the oscillation pattern of the photonic waveguide-mode and hybrid plasmonic mode more clearly, the electric field distributions of fundamental mode in the $y-z$ plane are calculated in Figure 2c,d. The calculated results of conventional photonic device demonstrate that the optical modes are mainly trapped inside the cavity body, leading to the formation of the resonant standing-wave propagating back and forth between the two end-facets of ZnO nanorod. Nevertheless, the fundamental mode electric field distribution of hybrid plasmonic nanolaser polarized in the z-direction is mainly confined and propagates in the crossover region, resulting in generation of nanometre-scale coherent optical fields and realization of ultracompact lasers. Also, some details of the fundamental and other multimode field distribution can be obtained in our simulation, as shown in Supporting Information, Figure S6.

Lasing Characterization of Plasmonic and Photonic Nanolasers. Figure 3 shows the representative spectra of photonic and plasmonic nanolasers pumped at a wavelength of 325 nm with 150 fs pulses at a repetition rate of 1000 Hz. Compared with the photonic lasing spectrum, an obviously blueshift of the plasmonic lasing can be observed in experiment. Generally, this optical phenomenon may be attributed to three reasons: (1) the different gain mechanism, (2) the quantum size effect, and (3) the Burstein–Moss (BM) effect. Here, ZnO gain medium of these two samples has a similar diameter, and the exciton density of the plasmonic device is generally lower than that of the photonic one analyzed through rate equation.[33,34] Therefore, we deduce that the blueshift that occurred in our case is mainly due to their different optical gain mechanisms of the conventional photonic and hybrid plasmonic lasers. To our knowledge, all reported photonic ZnO lasers have operated via the EHP mechanism, with emission energies near 3.20 eV,[35,36] which located in the blue regime marked in Figure 3. According to the absorption coefficient $\beta \approx 1.6 \times 10^5$ cm^{-1},[37,38] the carrier density in the traditional F–P resonant cavity can be estimated by $n_p = \beta \cdot I_{exc}/\hbar\omega_{exc}$. When I_{exc} is increased from 3.18 to 4.37 mJ/cm^2

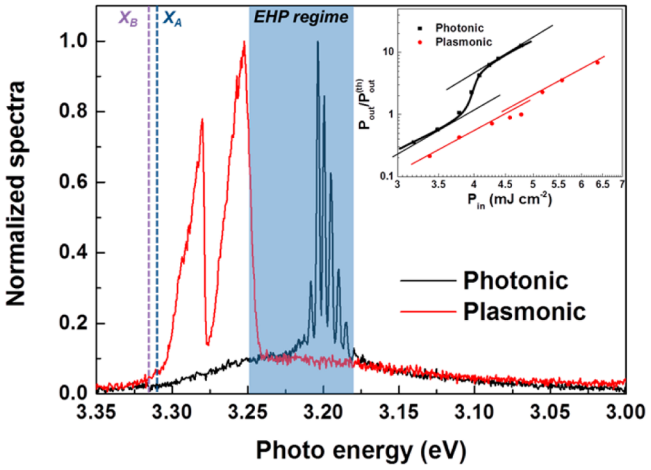

Figure 3. Comparison of measured plasmonic and photonic nanolaser emission. The inset shows laser light output (P_{out}) normalized to the threshold value ($P_{out}^{(th)}$) vs the optical pump energy density (P_{in}) for the plasmonic (red dot) and photonic (black dot) nanolasers. The dashed line labeled X_A, X_B and blue regime represent the ZnO exciton energies and the EHP energy range.

(Supporting Information, Figure S5), the carrier concentration n_p increases from 1.0×10^{21} cm^{-3} to 1.4×10^{21} cm^{-3}, which is far beyond the Mott density of ZnO ($\sim 10^{17}$ cm^{-3}).[35,39] Such a high carrier concentration definitely results in exciton dissociation into electron–hole plasma (EHP), which together with bandgap renormalization provides gain as far below the band-edge, leading to the generation of EHP lasing rather than the exciton lasing in the photonic ZnO nanolasers. However, the plasmonic lasing emission locates at the exciton energies of ZnO near 3.30 eV, which originates mainly from the two lowest energies (X_A, X_B labeled in Figure 3) of three excitons ($\hbar\omega_A$ = 3.309 eV, $\hbar\omega_B$ = 3.315 eV, and $\hbar\omega_C$ = 3.355 eV)[40] and their phonon replica energies ($\hbar\omega_{LO}$ = 72 meV) at room temperature. The constructed semiconductor–insulator–metal interface implements an effective energy-transfer channel of exciton–plasmon coupling, offering the sufficient optical gain from semiconductor to overcome the intrinsic metallic losses. Thus, the gain mechanisms of the photonic and plasmonic nanolasers are entirely different, where the former is attributed

DOI: 10.1021/acsphotonics.7b00476
ACS Photonics 2017, 4, 2419–2424

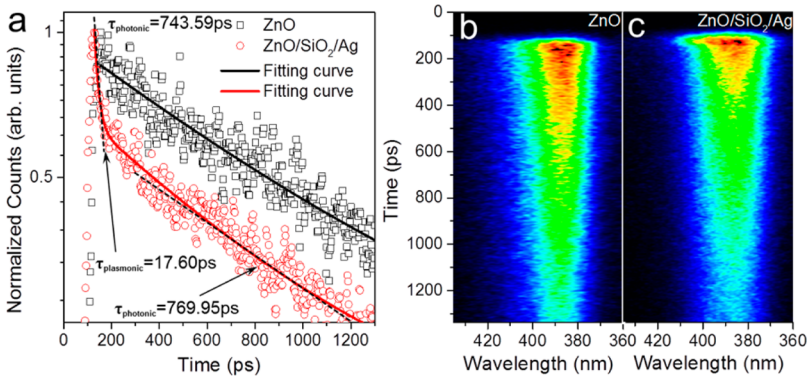

Figure 4. Exciton dynamics measured by time-resolved photoluminescence and Purcell factors. (a) Time-resolved spectral response collected from plasmonic (red dots) and photonic (black dots) samples, fitted by double and single-exponential function, respectively. Temporal spectroscopic profile of (b) ZnO/SiO_2 and (c) ZnO/SiO_2/Ag samples excited by 295 nm laser and collected by a streak camera.

to the EHP mechanism; meanwhile, the latter arises from the SPP-coupled exciton energy. The inset of Figure 3 shows laser light output (P_{out}) normalized to the threshold value ($P_{out}^{(th)}$) versus the optical pump energy density (P_{in}) for the plasmonic and photonic nanolasers. In general, plasmonic laser demonstrates a suppressed superlinear light versus pump response near the laser transition compared to photonic device, which is characteristic of enhanced spontaneous recombination arising from the mode localization and reduced mode competition.[41] The thresholds of the photonic and plasmonic lasers are 3.81 and 4.78 mJ/cm^2, respectively. The differences in threshold, electric field distribution, laser mode polarization, and lasing mode-shift suggest the role of SPP modes in the lasing action.

Excitonic Dynamic Processes of Plasmonic and Photonic Nanolasers. For more insights into the dynamic coupling processes, time-resolved photoluminescence (TRPL) measurements are performed at room temperature, as shown in Figure 4. The temporal spectroscopic profiles collected by a streak camera are shown in panels b and c of Figure 4. The normalized TRPL decays curves of the photonic and plasmonic samples can be fitting using the monoexponential and biexponential function well, respectively. The different decay lifetimes is defined as follows:[42,43]

$$I(t) = I_0 \exp(-t/\tau_{photonic}) \quad (1)$$

$$I(t) = I_1 \exp(-t/\tau_{photonic}) + I_2 \exp(-t/\tau_{plasmonic}) \quad (2)$$

where I_0, I_1, and I_2 are the fitting parameters. The calculated decay time of the photonic device is ~743.59 ps. The spontaneous emission decay rate of ZnO nanorod is significantly enhanced in the plasmonic device[44] compared with the photonic one[45] due to Purcell effect, indicating the accelerated the exciton recombination by coupling with SPPs of Ag. The enhanced decay rate in the plasmon-coupled device can be observed with two lifetimes of ~769.95 and ~17.60 ps, which is corresponding to the intrinsic and SP-coupled exciton recombination, respectively. Thus, the Purcell factor is estimated by up to 40 for the hybrid plasmonic device, implying the ultrafast energy-transfer process from excitons to SPs. In other words, the relatively lower exciton density under the Mott density can be predicted as the hybrid plasmonic device lase with the sufficient gain compensation obtained from the accelerated exciton recombination, thereby, revealing a totally different optical gain mechanism compared with that (EHP) of conventional photonic laser, as mentioned above.

CONCLUSIONS

We realized a hybrid plasmonic laser consisting of a high-gain ZnO nanorod, separated from a silver surface by a 5 nm thick insulating gap with a high Purcell factor up to 40. The calculated and experimental results demonstrated that the SPP modes play an important role in the lasing action, which will affect the lasing threshold, electric field distribution, laser mode polarization and lasing mode-shift. We proposed that the fundamental reason for lasing mode-shift is mainly derived from the different optical gain mechanism, which can be further confirmed by the analysis of the exciton recombination dynamics processes. Our study describes a clear physical model for the SPP-induced energy-transfer processes, and clarifies the exciton-SP coupling mechanism in the plasmonic nanolasers. These results provide a solid physical basis for the application of SPP nanolaser in the field of nanoscaled, all-optical integrated optoelectronic devices.

METHOD

Sample Preparation. To construct the photonic and plasmonic nanolaser, we fabricated ZnO nanorods as the gain medium on the Si substrate (Supporting Information, Figure S1) by the vapor-phase transport method described in ref 26. Also, 500 nm Ag and then 5 nm of SiO_2 were deposited on a Si/SiO_2 (300 nm thermal oxide) substrate by the magnetron sputtering technique. The sputtering time is estimated for lasting 10 min based on the deposition rate of SiO_2 (Supporting Information, Figure S2). The root-mean-square (RMS) roughness of SiO_2/Ag film is 4 nm (Supporting Information, Figure S3), which is much smaller than the diameter of ZnO nanorod. After that, the ZnO nanorods were wet-transferred from solution by dripping onto the deposited sample. The same technique was used to transfer nanorods onto the Si/SiO_2 substrate to construct photonic laser samples. Although the substrate materials of the two samples were chosen for practical reasons, the different refractive indexes do not influence optical mode confinement, as the nanorods are predominantly embedded in air.[27]

Optical Measurement Systems. To pump the plasmonic and photonic lasers, a mode-locked Ti-sapphire femtosecond (fs) laser (800 nm, Coherent Libra-F-HE) was employed as the seed beam. The excitation laser (λ_{ex} = 325 nm, repetition rate 1000 Hz, pulse length 150 fs) was generated by an optical parametric amplifier and focused onto the samples through an upright microscope (Olympus BX53). To measure the lasing

DOI: 10.1021/acsphotonics.7b00476
ACS Photonics 2017, 4, 2419−2424

spectra signals we detect nanorods emission by an optical multichannel analyzer (Princeton Instruments, Acton SP2500i) equipped with a CCD detector.

To measure the spectral-temporal response of our samples, time-resolved photoluminescence (TRPL) experiments were performed by using an optically triggered streak camera system (C10910, Hamamatsu) at 295 nm resulting from frequency doubling of the fundamental 35 fs pulses at 590 nm with a repetition rate of 1 kHz (OperA Solo, Coherent).

Simulation. To compare the properties of hybrid plasmonic mode and conventional photonic mode, the Finite Difference Time Domain (FDTD) software was employed to calculate the modal eigenvalues and the near-field electric field distribution. The effective index and propagation distance were determined from the real and imaginary parts of the eigenvalue solve. The refractive indices of ZnO and SiO_2 are 2.4 and 1.5 at λ = 375 nm, respectively. The dielectric function of silver refers to ref 28. In photonic mode simulation, the thickness of SiO_2 film is assumed to be infinite. For more details about numerical simulations, please see the Supporting Information.

■ ASSOCIATED CONTENT

Supporting Information

The Supporting Information is available free of charge on the ACS Publications website at DOI: 10.1021/acsphotonics.7b00476.

Details on morphology and structural characterization of ZnO, the deposition rate of $SiO_2$and RMS roughness, the simulated analysis on the plasmonic nanolasers with different spacer thickness and the electric field distribution of SPP wave transmission under the different modes, the spontaneous emission of ZnO nanorods, and the stimulated emission under different excitation power and spectral analysis (PDF).

■ AUTHOR INFORMATION

Corresponding Author

*E-mail: xcxseu@seu.edu.cn.

ORCID

Junfeng Lu: 0000-0001-6458-7734
Mingming Jiang: 0000-0003-1784-582X
Chunxiang Xu: 0000-0001-8116-2869
Caofeng Pan: 0000-0001-6327-9692

Author Contributions

§These authors contributed equally to this work.

Notes

The authors declare no competing financial interest.

■ ACKNOWLEDGMENTS

This work was supported by National Natural Science Foundation of China (61475035, 61275054, 11404328, and 11574307), National Basic Research Program of China (2013CB932903), and Science and Technology Project of Jiangsu Province (BE2016177). Also, we thank the help of collaborative Innovation Center of Suzhou Nano Science and Technology.

■ REFERENCES

(1) Kretschmann, E.; Raether, H. Radiative Decay of Nonradiative Surface Plasmons Excited by Light. *Z. Naturforsch., A: Phys. Sci.* **1968**, *23* (12), 2135−2136.

(2) Otto, A. Excitation of Nonradiative Surface Plasma Waves in Silver by the Method of Frustrated Total Reflection. *Z. Phys. A: Hadrons Nucl.* **1968**, *216* (4), 398−410.

(3) Barnes, W. L.; Dereux, A.; Ebbesen, T. W. Surface Plasmon Subwavelength Optics. *Nature* **2003**, *424* (6950), 824−830.

(4) Williams, B. S. Terahertz Quantum Cascade Lasers. *Nat. Photonics* **2007**, *1*, 517−525.

(5) Almeida, V. R.; Barrios, C. A.; Panepucci, R. R.; Lipson, M. All-optical Control of Light on a Silicon Chip. *Nature* **2004**, *431*, 1081−1084.

(6) Sorger, V. J.; Ye, Z. L.; Oulton, R. F.; Wang, Y.; Bartal, G.; Yin, X. B.; Zhang, X. Experimental Demonstration of Low-loss Optical Waveguiding at Deep Sub-wavelength Scales. *Nat. Commun.* **2011**, *2*, 331.

(7) Nie, S. M.; Emory, S. R. Probing Single Molecules and Single Nanoparticles by Surface-enhanced Raman Scattering. *Science* **1997**, *275* (5303), 1102−1106.

(8) Anker, J. N.; Hall, W. P.; Lyandres, O.; Shah, N. C.; Zhao, J.; Duyne, R. P. V. Biosensing with plasmonic nanosensors. *Nat. Mater.* **2008**, *7*, 442−453.

(9) Lu, J. F.; Xu, C. X.; Nan, H. Y.; Zhu, Q. X.; Qin, F. F.; Manohari, A. G.; Wei, M.; Zhu, Z.; Shi, Z. L.; Ni, Z. H. SERS-active ZnO/Ag Hybrid WGM Microcavity for Ultrasensitive Dopamine Detection. *Appl. Phys. Lett.* **2016**, *109*, 073701.

(10) Yu, Z.; Veronis, G.; Fan, S.; Brongersma, M. L. Gain-induced Switching in Metal-dielectric-metal Plasmonic Waveguides. *Appl. Phys. Lett.* **2008**, *92*, 041117.

(11) Ma, R. M.; Oulton, R. F.; Sorger, V. J.; Bartal, G.; Zhang, X. Room-temperature sub-diffraction-limited plasmon laser by total internal reflection. *Nat. Mater.* **2011**, *10* (2), 110−113.

(12) Noginov, M. A.; Zhu, G.; Belgrave, A. M.; Bakker, R.; Shalaev, V. M.; Narimanov, E. E.; Stout, S.; Herz, E.; Suteewong, T.; Wiesner, U. Demonstration of a Spaser-based Nanolaser. *Nature* **2009**, *460* (7259), 1110−1112.

(13) Berini, P.; De Leon, I. Surface Plasmon-polariton Amplifiers and Lasers. *Nat. Photonics* **2011**, *6* (1), 16−24.

(14) Hill, M. T.; Oei, Y. S.; Smalbrugge, B.; Zhu, Y. C.; Vries, T. D.; Veldhoven, P. J. V.; Otten, F. W. M. V.; Eijkemans, T. J.; Turkiewicz, J. P.; Waardt, H. D.; Geluk, E. J.; Kwon, S. H.; Lee, Y. H.; Nötzel, R.; Smit, M. K. Lasing in metallic-coated nanocavities. *Nat. Photonics* **2007**, *1*, 589−594.

(15) Hill, M. T.; Marell, M.; Leong, E. S. P.; Smalbrugge, B.; Zhu, Y.; Sun, M.; Veldhoven, P. J.V.; Geluk, E. J.; Karouta, F.; Oei, Y. S.; Nötzel, R.; Ning, C. Z.; Smit, M. K. Lasing in Metal-insulator-metal Sub-wavelength Plasmonic Waveguides. *Opt. Express* **2009**, *17*, 11107−11112.

(16) Kwon, S. H.; Kang, J. H.; Seassal, C.; Kim, S. K.; Regreny, P.; Lee, Y. H.; Lieber, C. M.; Park, H. G. Subwavelength Plasmonic Lasing from a Semiconductor Nanodisk with Silver Nanopan Cavity. *Nano Lett.* **2010**, *10*, 3679−3683.

(17) Khajavikhan, M.; Simic, A.; Lee, K. J. H.; Slutsky, B.; Mizrahi, A.; Lomakin, V.; Fainman, Y. Thresholdless Nanoscale Coaxial Lasers. *Nature* **2012**, *482*, 204−207.

(18) Ding, K.; Liu, Z. C.; Yin, L. J.; Hill, M. T.; Marell, M. J. H.; Veldhoven, P. J. V.; Nöetzel, R.; Ning, C. Z. Room-temperature Continuous Wave Lasing in Deep-subwavelength Metallic Cavities under Electrical Injection. *Phys. Rev. B: Condens. Matter Mater. Phys.* **2012**, *85*, 041301.

(19) Kevin, C. Y.; Huang, M. K. S.; Sarmiento, T.; Huo, Y. J.; Harris, J. S.; Brongersma, M. L. Electrically Driven Subwavelength Optical Nanocircuits. *Nat. Photonics* **2014**, *8* (3), 244−249.

(20) Oulton, R. F.; Sorger, V. J.; Genov, D. A.; Pile, D. F. P.; Zhang, X. A Hybrid Plasmonic Waveguide for Subwavelength Confinement and Long-range Propagation. *Nat. Photonics* **2008**, *2* (8), 496−500.

(21) Oulton, R. F.; Sorger, V. J.; Zentgraf, T.; Ma, R. M.; Gladden, C.; Dai, L.; Bartal, G.; Zhang, X. Plasmon Lasers at Deep Subwavelength Scale. *Nature* **2009**, *461* (7264), 629−632.

DOI: 10.1021/acsphotonics.7b00476
ACS Photonics 2017, 4, 2419−2424

(22) Zhang, Q.; Li, G. Y.; Liu, X. F.; Qian, F.; Li, Y.; Sum, T. C.; Lieber, C. M.; Xiong, Q. H. A Room Temperature Low-threshold Ultraviolet Plasmonic Nanolaser. *Nat. Commun.* **2014**, *5*, 4953.
(23) Chou, Y. H.; Wu, Y. M.; Hong, K. B.; Chou, B. T.; Shih, J. H.; Chung, Y. C.; Chen, P. Y.; Lin, T. R.; Lin, C. C.; Lin, S. D.; Lu, T. C. High-Operation-Temperature Plasmonic Nanolasers on Single-Crystalline Aluminum Crystalline Aluminum. *Nano Lett.* **2016**, *16*, 3179−3186.
(24) Sidiropoulos, T. P. H.; Röder, R.; Geburt, S.; Hess, O.; Maier, S. A.; Ronning, C.; Oulton, R. F. Ultrafast Plasmonic Nanowire Lasers near the Surface Plasmon Frequency. *Nat. Phys.* **2014**, *10* (11), 870−876.
(25) Liu, X. F.; Zhang, Q.; Yip, J. N.; Xiong, Q. H.; Sum, T. C. Wavelength Tunable Single Nanowire Lasers Based on Surface Plasmon Polariton Enhanced Burstein-Moss Effect. *Nano Lett.* **2013**, *13* (11), 5336−5343.
(26) Li, J. T.; Lin, Y.; Lu, J. F.; Xu, C. X.; Wang, Y. Y.; Shi, Z. L.; Dai, J. Single Mode ZnO Whispering-Gallery Submicron Cavity and Graphene Improved Lasing Performance. *ACS Nano* **2015**, *9* (7), 6794−6800.
(27) Zimmler, M. A.; Capasso, F.; Müller, S.; Ronning, C. Optically Pumped Nanowire Lasers: Invited Review. *Semicond. Sci. Technol.* **2010**, *25*, 024001.
(28) Johnson, P. B.; Christy, R. W. Optical Constants of the Noble Metals. *Phys. Rev. B* **1972**, *6* (12), 4370−4379.
(29) Lu, J. F.; Xu, C. X.; Dai, J.; Li, J. T.; Wang, Y. Y.; Lin, Y.; Li, P. L. Improved UV Photoresponse of ZnO Nanorod Arrays by Resonant Coupling with Surface Plasmons of Al Nanoparticles. *Nanoscale* **2015**, *7*, 3396−3403.
(30) Ding, H. Y.; Zhao, Z.; Zhang, G. H.; Wu, Y. K.; Gao, Z. W.; Li, J. W.; Zhang, K.; Pan, N.; Wang, X. P. Oxygen Vacancy: An Electron-Phonon Interaction Decoupler to Modulate the Near-Band-Edge Emission of ZnO Nanorods. *J. Phys. Chem. C* **2012**, *116* (32), 17294−17299.
(31) Shih, T.; Mazur, E.; Richters, J. P.; Gutowski, J.; Voss, T. Ultrafast Exciton Dynamics in ZnO: Excitonic versus Electron-hole Plasma Lasing. *J. Appl. Phys.* **2011**, *109*, 043504.
(32) Klingshirn, C. ZnO: Material, physics and applications. *ChemPhysChem* **2007**, *8*, 782−803.
(33) Chou, Y. H.; Chou, B. T.; Chiang, C. K.; Lai, Y. Y.; Yang, C. T.; Li, H.; Lin, T. R.; Lin, C. C.; Kuo, H. C.; Wang, S. C.; Lu, T. C. Ultrastrong Mode Confinement in ZnO Surface Plasmon Nanolasers. *ACS Nano* **2015**, *9* (4), 3978−3983.
(34) Gao, H. W.; Fu, A.; Andrews, S. C.; Yang, P. D. Cleaved-coupled nanowire lasers. *Proc. Natl. Acad. Sci. U. S. A.* **2013**, *110* (3), 865−869.
(35) Versteegh, M. A. M.; Vanmaekelbergh, D.; Dijkhuis, J. I. Room-temperature Laser Emission of ZnO Nanowires Explained by Many-body Theory. *Phys. Rev. Lett.* **2012**, *108*, 157402.
(36) Kwok, W. M.; Djurišić, A. B.; Leung, Y. H.; Chan, W. K.; Phillips, D. L. Time-resolved Photoluminescence Study of the Stimulated Emission in ZnO Nanoneedles. *Appl. Phys. Lett.* **2005**, *87* (9), 093108.
(37) Fallert, J.; Dietz, R. J. B.; Sartor, J.; Schneider, D.; Klingshirn, C.; Kalt, H. Co-existence of strongly and weakly localized random laser modes. *Nat. Photonics* **2009**, *3* (5), 279−282.
(38) Muth, J. F.; Kolbas, R. M.; Sharma, A. K.; Oktyabrsky, S.; Narayan, J. Excitonic Structure and Adsorption Coefficient Measurements of ZnO Single Crystal Epitaxial Films Deposited by Pulsed Laser Deposition. *J. Appl. Phys.* **1999**, *85* (11), 7884−7887.
(39) Dai, J.; Xu, C. X.; Nakamura, T.; Wang, Y. Y.; Li, J. T.; Lin, Y. Electron-hole Plasma Induced Band Gap Renormalization in ZnO Microlaser Cavities. *Opt. Express* **2014**, *22* (23), 28831−28837.
(40) Yoshikawa, H.; Adachi, S. Optical Constants of ZnO. Jpn. *J. Appl. Phys.* **1997**, *36*, 6237−6243.
(41) Ma, R. M.; Oulton, R. F.; Sorger, V. J.; Zhang, X. Plasmon Lasers: Coherent Light Source at Molecular Scales. *Laser Photonics Rev.* **2013**, *7* (1), 1−21.
(42) Lu, J. F.; Shi, Z. L.; Wang, Y. Y.; Lin, Y.; Zhu, Q. X.; Tian, Z. S.; Dai, J.; Wang, S. F.; Xu, C. X. Plasmon-enhanced Electrically Light-emitting from ZnO Nanorod Arrays/p-GaN Heterostructure Devices. *Sci. Rep.* **2016**, *6*, 25645.
(43) Oulton, R. F. Surface Plasmon Lasers: Sources of Nanoscopic Light. *Mater. Today* **2012**, *15* (1), 26−34.
(44) Li, G. Y.; Liu, X. F.; Wang, X. Z.; Yuan, Y. W.; Sum, T. C.; Xiong, Q. H. Purified plasmonic lasing with strong polarization selectivity by reflection. *Opt. Express* **2015**, *23* (12), 15657−15669.
(45) Li, G. Y.; Xiong, Q. H. Scattering by abrupt discontinuities on photonic nanowires: closed-form expressions for domain reduction. *Opt. Express* **2014**, *22* (21), 25137−25148.

DOI: 10.1021/acsphotonics.7b00476
ACS Photonics 2017, 4, 2419−2424